

Standard electroweak theory predicts a single fundamental scalar particle, the Higgs boson, which arises as a result of spontaneous electroweak symmetry breaking [1]; however, the Higgs boson has not been directly observed experimentally. It is in fact the only fundamental standard model particle which has not been observed. The current direct experimental constraint on the Higgs boson mass, $m_H > 114.4 \text{ GeV}/c^2$ at 95% confidence level (C.L.), comes from direct Higgs boson searches at LEP2 experiments [2]. Global fits to electroweak measurements and LEP2 experiments combined results exclude masses above $185 \text{ GeV}/c^2$ at 95% CL [3].

At the Tevatron $p\bar{p}$ collider at Fermilab, the next-to-leading-order (NLO) Higgs boson production cross section prediction is about 10 times larger for gluon fusion than for WH associated production, and the cross section for WH is about twice that of ZH [4]. The Higgs boson decay branching fraction is dominated by $H \rightarrow b\bar{b}$ for $m_H < 135 \text{ GeV}/c^2$ and by $H \rightarrow W^+W^-$ for $m_H > 135 \text{ GeV}/c^2$ [5]. Background QCD $b\bar{b}$ production processes have cross sections at least four orders of magnitude greater than that of Higgs boson production [6], and this renders searches in the $gg \rightarrow H \rightarrow b\bar{b}$ channel unviable. However, requiring the leptonic decay of the associated W boson reduces the huge QCD background rate. As a result, $WH \rightarrow \ell\nu b\bar{b}$ is considered to be one of the most sensitive processes for low mass Higgs boson searches ¹.

Searches for $WH \rightarrow \ell\nu b\bar{b}$ at $\sqrt{s} = 1.96 \text{ TeV}$ have been most recently reported by CDF (using data corresponding to an integrated luminosity of 955 pb^{-1}) [7, 8] and D0 (440 pb^{-1}) [9]. In this paper, we present an update search for $WH \rightarrow \ell\nu b\bar{b}$ production at CDF using about 1.9 fb^{-1} of data and improved analysis techniques. To increase the acceptance for double b -tagged events, we introduce another b -tagging algorithm, jet probability b -tagging, which uses the impact parameter information of tracks inside jets. In addition we increase the signal acceptance by including the electrons going into the forward region of the detector and introduce a multivariate discriminant technique using a neural network (NN) to reduce large background contamination after event selection.

The paper is organized as follows. Section II describes the CDF II detector. The event selection criteria are explained in Sec. III. In Sec. IV the b -tagging algorithms with SECVTX, b -tagging filter, and Jet Probability are discussed in detail. Contributions from the standard

¹ In this paper, lepton (ℓ) denotes electron (e^\pm) or muon (μ^\pm), and neutrino (ν) denotes electron neutrino (e_ν) or muon neutrino (μ_ν).

37 model (SM) background are calculated in Sec. V for various sources. In Sec. VI, signal
 38 acceptance and systematic uncertainties are estimated. The Neural Network discriminant
 39 technique is described in Sec. VII. The results and statistical interpretation of the results
 40 are presented in Secs. VIII. Finally, our conclusions are presented in Sec. X.

41 II. CDF II DETECTOR

42 The CDF II detector geometry is described using a cylindrical coordinate system [10].
 43 The z -axis follows the proton direction, and the polar angle θ is usually expressed through
 44 the pseudorapidity $\eta = -\ln(\tan(\theta/2))$. The detector is approximately symmetric in η and in
 45 the azimuthal angle ϕ . The transverse energy is defined as $E_T = E \sin \theta$, and the transverse
 46 momentum $p_T = p \sin \theta$.

47 Charged particles are tracked by a system of silicon microstrip detectors and a large open
 48 cell drift chamber in the region $|\eta| \leq 2.0$ and $|\eta| \leq 1.0$, respectively. The tracking detectors
 49 are immersed in a 1.4 T solenoidal magnetic field aligned coaxially with the incoming beams,
 50 allowing measurement of charged particle momentum transverse to the beamline (p_T).

51 The transverse momentum resolution is measured to be $\delta p_T/p_T \approx 0.1\% \cdot p_T(\text{GeV})$ for the
 52 combined tracking system. The resolution on the track impact parameter (d_0), or distance
 53 from the beamline axis to the track at the track's closest approach in the transverse plane,
 54 is $\sigma(d_0) \approx 40 \mu\text{m}$, of which about $30 \mu\text{m}$ is due to the transverse size of the Tevatron beam
 55 itself.

56 Outside of the tracking systems and the solenoid, segmented calorimeters with projective
 57 tower geometry are used to reconstruct electromagnetic showers and hadronic jets [11–13]
 58 over the pseudo-rapidity range $|\eta| < 3.6$. A transverse energy is measured in each calorimeter
 59 tower where the polar angle (θ) is calculated using the measured z position of the event vertex
 60 and the tower location.

61 Small contiguous groups of calorimeter towers with signals are identified and summed
 62 together into an energy cluster. Electron candidates are identified in the central electromag-
 63 netic calorimeter (CEM) or in the forward, known as the plug, electromagnetic calorimeter
 64 (PEM) as isolated, mostly electromagnetic clusters that match a track in the pseudorapidity
 65 range $|\eta| < 1.1$ and $|\eta| < 2.0$, respectively. The electron transverse energy is reconstructed
 66 from the electromagnetic cluster with a precision $\sigma(E_T)/E_T = 13.5\%/\sqrt{E_T/(\text{GeV})} \oplus 2\%$

67 for central [11] and $\sigma(E_T)/E_T = 16.0\%/\sqrt{E_T}/(\text{GeV}) \oplus 2\%$ for plug. Jets are identi-
68 fied as a group of electromagnetic (EM) and hadronic calorimeter clusters (HAD) which
69 fall within a cone of radius $\Delta R = \sqrt{\Delta\phi^2 + \Delta\eta^2} \leq 0.4$ units around a high- E_T seed clus-
70 ter [14]. Jet energies are corrected for calorimeter non-linearity, losses in the gaps be-
71 tween towers and multiple primary interactions. The jet energy resolution is approximately
72 $\sigma(E_T) = [0.1E_T/(\text{GeV}) + 1.0] \text{ GeV}$ [15].

73 For this analysis, muon candidates are detected in three separate subdetectors. After
74 at least five interaction lengths in the calorimeter, the muons first encounter four layers
75 of planar drift chambers (CMU), capable of detecting muons with $p_T > 1.4 \text{ GeV}/c$ [16].
76 Four additional layers of planar drift chambers (CMP) behind another 60 cm of steel detect
77 muons with $p_T > 2.8 \text{ GeV}/c$ [17]. These two systems cover the same central pseudorapidity
78 region with $|\eta| \leq 0.6$. Muons that exit the calorimeters at $0.6 \leq |\eta| \leq 1.0$ are detected by
79 the CMX system of four drift layers. Muon candidates are then identified as isolated tracks
80 which extrapolate to line segments or “stubs” in one of the muon subdetectors. A track that
81 is linked to both CMU and CMP stubs is called a CMUP muon.

82 The missing transverse energy (\cancel{E}_T) is a reconstructed quantity that is defined as the
83 opposite of the vector sum of all calorimeter tower energy depositions projected on the
84 transverse plane. It is often used as a measure of the sum of the transverse momenta of the
85 particles that escape detection, most notably neutrinos. To be more readily interpretable as
86 such, the raw \cancel{E}_T vector is adjusted for corrected jet energies and for the energy deposition
87 of any minimum ionizing high- p_T muons.

88 The CDF trigger system is a three-level filter, with tracking information available at
89 the first level [18]. Events used in this analysis have all passed the high-energy electron
90 or muon trigger selection. The first stage of the central electron trigger requires a track
91 with $p_T > 8 \text{ GeV}/c$ pointing to a tower with $E_T > 8 \text{ GeV}$ and $E_{\text{HAD}}/E_{\text{EM}} < 0.125$. The
92 plug electron (MET+PEM) trigger requires a tower with $E_T > 8 \text{ GeV}$, $E_{\text{HAD}}/E_{\text{EM}} < 0.125$
93 and the missing transverse energy (\cancel{E}_T) $> 15 \text{ GeV}$. The first stage of the muon trigger
94 requires a track with $p_T > 4 \text{ GeV}/c$ (CMUP) or $8 \text{ GeV}/c$ (CMX) pointing to a muon stub.
95 A complete lepton reconstruction is performed online in the final trigger stage, where we
96 require $E_T > 18 \text{ GeV}$ for central electrons (CEM), $E_T > 18 \text{ GeV}$ and $\cancel{E}_T > 20 \text{ GeV}$ for
97 MET+PEM and $p_T > 18 \text{ GeV}/c$ for muons (CMUP,CMX).

99 The results presented here use data collected between February 2002 and May 2007.
 100 The data collected using the CEM, CMUP and MET+PEM triggers correspond to $1.92 \pm$
 101 0.12 fb^{-1} , while the data from the CMX trigger corresponds to $1.88 \pm 0.11 \text{ fb}^{-1}$.

102 The observable final state from the $WH \rightarrow \ell\nu b\bar{b}$ signal consists of two b -jets plus a lepton
 103 and missing transverse energy. The leptonic W decay requirement in WH events yields the
 104 high- p_T lepton and large missing transverse energy due to the neutrino.

105 Events are considered as WH candidates only if they have exactly one high- p_T isolated
 106 lepton candidate [19], with $E_T > 20 \text{ GeV}$ for electrons or $p_T > 20 \text{ GeV}/c$ for muons. The
 107 isolation cone of $\Delta R = 0.4$ surrounding the lepton must have less than 10% of the lepton
 108 energy. A primary event vertex position is calculated by fitting a subset of particle tracks
 109 that are consistent with having come from the beamline. The distance between this primary
 110 event vertex and the lepton track z_0 must be less than 5 cm to ensure the lepton and the
 111 jets come from the same hard interaction. Some leptonic Z decays would mimic the single-
 112 lepton signature if a lepton is unidentified. Events are therefore rejected if a second track
 113 with $p_T > 10 \text{ GeV}/c$ forms an invariant mass with the lepton that falls in the Z -boson mass
 114 window ($76 < m_{\ell X} < 106 \text{ GeV}/c^2$). The selected events are required to have \cancel{E}_T greater
 115 than 20 GeV.

116 In the plug region, we require a high- p_T isolated lepton candidate with $E_T > 20 \text{ GeV}$,
 117 where the selection criteria are the same as for the central region, except for an imposed
 118 more tightly \cancel{E}_T requirement because of the much higher QCD contamination. To reduce
 119 contributions from QCD events, the following criteria are imposed: $MET_{sig} > 2$, $\cancel{E}_T > 25$
 120 GeV and $\cancel{E}_T > 45 \text{ GeV}$ when the \cancel{E}_T is pointing close to a jet, and large transverse mass of
 121 the reconstructed W , $M_T(W) > 20 \text{ GeV}/c^2$. Here, MET_{sig} is defined as the ratio of \cancel{E}_T to
 122 a weighted sum of factors correlated with mismeasurement, such as angles between the \cancel{E}_T
 123 and the jet and amount of jet energy corrections, and $M_T(W)$ is defined as follows:

$$124 \quad M_T(W) = \sqrt{2p_T^{lep}\cancel{E}_T - \mathbf{p}_T^{lep} \cdot \cancel{\mathbf{E}}_T}.$$

125 The WH signal includes two jets originating from $H \rightarrow b\bar{b}$ decays; these jets are expected
 126 to have large transverse energy. The jets are required to be in the pseudorapidity range
 127 covered by the silicon detector so that secondary vertices from b decays can be reconstructed.

128 Specifically, we require the jets satisfy $E_T > 20$ GeV and $|\eta| < 2.0$. The search for $WH \rightarrow$
129 $\ell\nu b\bar{b}$ is performed in the sample of events with W + exactly 2 jets; however, samples of events
130 with $W+1,3,\geq 4$ jets are used to cross-check the background modeling.

131 To increase the signal purity of the $W+2$ -jet events, at least one jet must be b -tagged
132 by the SECVTX algorithm. Three exclusive b -tagged event categories are considered. The
133 first category (ST+ST) is for events where there are two SECVTX b -tagged jets. The second
134 category (ST+JP) consists of events where only one of the jets is b -tagged by the SECVTX
135 and the second jet is b -tagged by jet probability. The third category (ST with NN filter)
136 contains events where only one of the jets is b -tagged by the SECVTX and also passes the
137 neural network b -tagging filter.

138 IV. b JET IDENTIFICATION ALGORITHM

139 The b -quark has a relatively long lifetime, and B hadrons formed during the hadronization
140 of the initial b quark can travel a significant distance before decaying into a collection of
141 lighter hadrons. The jets containing b -quark decay can be reconstructed by identifying tracks
142 significantly displaced from the $p\bar{p}$ interaction point (primary vertex).

143 Multijet final states have dominant contributions from QCD light flavor jet production,
144 but the standard model Higgs boson decays predominantly to bottom quark pairs. Correctly
145 identifying the b quark jets helps to remove most of the QCD background. In this analysis,
146 we introduce some b -identification algorithms to optimize the selection of b -quark jets.

147 A. Secondary Vertex b -Tagging

148 The SECVTX b -tagging algorithm is applied to each jet in the event, using only the tracks
149 which are within η - ϕ distance of $\Delta R = 0.4$ of the jet direction. Displaced tracks in jets
150 are used for the SECVTX reconstruction and are distinguished by a large impact parameter
151 significance ($|d_0/\sigma_{d_0}|$) where d_0 and σ_{d_0} are the impact parameter and the total uncertainty
152 from tracking and beam position measurements. Secondary vertices are reconstructed with
153 a two-pass approach which tests for high-quality vertices in the first pass and allows lower-
154 quality vertices in the second pass. In pass 1, at least three tracks are required to pass
155 loose selection criteria ($p_T > 0.5$ GeV/ c , $|d_0/\sigma_{d_0}| > 2.0$), and a secondary vertex is fit

156 from the selected tracks. One of the tracks used in the reconstruction is required to have
 157 $p_T > 1.0 \text{ GeV}/c$. If pass 1 fails, then a vertex is sought in pass 2 from at least two tracks
 158 satisfying tight selection criteria ($p_T > 1.0 \text{ GeV}/c$, $|d_0/\sigma_{d_0}| > 3.5$ and one of the pass 2 tracks
 159 must have $p_T > 1.5 \text{ GeV}/c$). If either pass is successful, the transverse distance (L_{xy}) from
 160 the primary vertex of the event is calculated along with the associated uncertainty. This
 161 uncertainty $\sigma_{L_{xy}}$ includes the uncertainty on the primary vertex position. Finally jets are
 162 tagged positively or negatively depending on the L_{xy} significance ($L_{xy}/\sigma_{L_{xy}}$):

$$163 \quad L_{xy}/\sigma_{L_{xy}} \geq 7.5 \quad (\text{positive tag}) \quad (1)$$

$$164 \quad L_{xy}/\sigma_{L_{xy}} \leq -7.5 \quad (\text{negative tag}) \quad (2)$$

165 These values have been tuned for optimum efficiency and purity in simulated b -jet samples
 166 from decays of top quarks. The energy spectrum for those jets is similar to the spectrum
 167 for b jets from decays of Higgs bosons.

168 The sign of L_{xy} indicates the position of the secondary vertex with respect to the primary
 169 vertex along the direction of the jet. If the angle between the jet axis and the vector pointing
 170 from the primary vertex to the secondary vertex is less than $\pi/2$, L_{xy} is positively defined;
 171 otherwise, it is negative. If L_{xy} is positive, the secondary vertex points towards the direction
 172 of the jet, as in true B hadron decays. For negative L_{xy} the secondary vertex points away
 173 from the jet; this may happen as a result of mismeasured tracks, so jets tagged with a
 174 negative L_{xy} are labeled mistagged jets. In order to reject secondary vertices due to material
 175 interaction, the algorithm vetoes two-track vertices found between 1.2 and 1.5 cm from the
 176 center of the silicon detector (the inner radius of the beampipe and the outer radius of the
 177 innermost silicon layer being within this range). All vertices more than 2.5 cm from the
 178 center are rejected.

179 The negative tags are useful for evaluating the rate of false positive tags, which are
 180 identified as “mistags” in the background estimates. Mismeasurements are expected to
 181 occur randomly; therefore the L_{xy} distribution of fake tags is expected to be symmetric
 182 with respect to zero. Simulated events are used to correct a small asymmetry due to true
 183 long-lived particles in light flavor jets.

184 The efficiency for identifying a secondary vertex is different in the simulated and observed
 185 datasets. We measure an efficiency scale factor, which is defined as the ratio of the observed
 186 to the simulated efficiencies, to be 0.95 ± 0.04 in a sample of high- E_T jets enriched in b jets

187 by requiring a soft lepton ($p_T > 8 \text{ GeV}/c$) from semileptonic heavy quark decays [20].

188 **B. Neural Network b -Tagging Filter**

189 An algorithm has been developed and used to tag displaced secondary vertices from b
190 quark decays; however, the sample tagged by the SECVTX algorithm still has significant
191 contamination from falsely-tagged light-flavor or gluon jets and the misidentification of c
192 quarks as b -jets [21]. This search uses a multivariate neural network technique intended to
193 improve the SECVTX tagging purity [7, 8].

194 The neural network used in this article employs the JETNET[22] package. The tagger is
195 designed with two networks in series. The $b - l$ network is trained to separate b -jets from
196 light-quark jets (l -jets), and the $b - c$ network is trained to separate b -jets from c -jets. Jets
197 that pass a cut on both of the NN outputs are accepted by the tagger. These neural networks
198 are trained and applied only to jets that are already tagged by the SECVTX algorithm. The
199 current NN b -tagging is tuned to increase the purity of the SECVTX b -tagged jets, not to
200 increase the tagging efficiency.

201 The neural networks take as input the 16 variables that are chosen primarily because the
202 b -quark jets have higher track multiplicity, larger invariant mass, longer lifetime and a harder
203 fragmentation function than c - and l -quarks jets. The track parameters and L_{xy} significance
204 are good discriminators for b -jets. The transverse momentum p_T^{vtx} and mass M_{vtx} of vertex
205 are useful variables for identifying l -jets; however c -jets have p_T spectra similar to b -jets.
206 Pseudo- $c\tau$ ($L_{xy} \times M_{\text{vtx}}/p_T^{\text{vtx}}$), the vertex fit χ^2 , and the track-based probability of a jet to
207 come from the primary vertex are the best discriminators.

208 The NN b -tagger is further validated by comparing the performance on a b -enriched
209 sample of SECVTX tagged heavy-flavor jets from events with an electron candidate with $E_T >$
210 8 GeV electron data and from the corresponding Monte Carlo sample. A good agreement is
211 found in NN b -tagger performance between data and Monte Carlo [7, 8].

212 The output of the neural net is a value ranging from 0 and 1 that can be tuned to
213 reject 65% of light-flavor jets and about 50% of the c jets while keeping 90% of b -jets after
214 being tagged by SECVTX. The data-to-Monte-Carlo scale factor, measured from the electron
215 sample, is 0.97 ± 0.02 . Note that this is an additional scale factor with respect to the SECVTX
216 efficiency scale factor because all of the jets under consideration have already been tagged

218 **C. Jet Probability b -tagging**

219 The jet probability b -tagging algorithm distinguishes itself by employing the signed im-
 220 pact parameters, and their uncertainties, of tracks in jets and calculates the probability that
 221 the jet was produced at a position consistent with the primary vertex. The sign of impact
 222 parameter is defined according to the angle ϕ between the jet axis and the direction to the
 223 track's closest point of approach with respect to the primary vertex. The sign is positive
 224 (negative) if $\cos \phi > 0 (< 0)$. A feature of this algorithm is that the b -tagging is performed
 225 using a continuous variable instead of a discrete object like a reconstructed secondary vertex.

226 For a light-quark jet, all particles should originate from the primary vertex. Due to the
 227 finite tracking resolution, these tracks are reconstructed with a non-zero impact parameter
 228 and have an equal probability to be either positive or negative signed. Since a long lived
 229 particle will travel some distance along the jet direction before decaying, its decay products
 230 will preferentially have positive signed impact parameters.

231 To calculate the jet probability value, the tracking resolution can be extracted from the
 232 inclusive jets data by fitting the negative side of the signed impact parameter distribution
 233 obtained for prompt jets. Tracks are sorted into different categories (η , p_T of tracks, and
 234 quality of silicon detector hits) to parametrize their properties. To minimize the contribution
 235 from badly measured tracks with large reconstructed impact parameters, the distribution of
 236 a related quantity, the signed impact parameter significance S_{d_0} (ratio of the signed impact
 237 parameter to its uncertainty) is parametrized at each track category. The impact parameter
 238 significance for each track is required to satisfy the quality criteria such as $p_T > 0.5\text{GeV}/c$
 239 and enough number of hits in tracking detector .

240 The resolution function is used to determine the track probability, which should be flat
 241 between 0 and 1 for tracks with a negative signed impact parameter because its distribution
 242 should be the same as the distribution used for obtaining the fitted function. For the tracks
 243 originating from long-lived particles with large positive signed impact parameter, the track
 244 probability has a peak near zero.

245 To calculate jet probability, at least two tracks with positive impact parameter are re-
 246 quired as the taggable condition. By definition, the jet probability distribution should be

247 flat for jets having only prompt tracks. Tracks with a negative impact parameter are used
 248 to define a negative P_{jet} , which is used to check the algorithm and to estimate the misiden-
 249 tification rate. We choose an operation point whereby the fake rate becomes about 5%.
 250 At this point, the b -tagging efficiency is about 60%. The difference between the simulated
 251 and observed data is taken into account as a scale factor. We measure the scale factor to
 252 be 0.85 ± 0.07 in a sample of high- E_T jets enriched in b jets by requiring a soft lepton from
 253 semileptonic heavy flavor decay. A more detailed description of the scale factor estimation
 254 is given in Ref. [23].

255 V. BACKGROUND

256 The final state signature of $WH \rightarrow \ell\nu b\bar{b}$ production can also be mimicked by other
 257 processes. The dominant background processes are W +jets production, $t\bar{t}$ production, and
 258 non- W QCD multijet production. Several electroweak production processes also contribute
 259 but with smaller rates. In the following subsections the contribution from each background
 260 source is discussed in detail. These background estimations are based on the same strategies
 261 used in the previous analysis [7, 8]. The summary of background estimate can be found in
 262 Sec. VIII.

263 A. Non- W QCD Multijet

264 Events from QCD multijet production sometimes mimic the W -boson signature by pro-
 265 ducing fake leptons or fake E_T . Non- W leptons are reconstructed when a jet passes the
 266 lepton selection criteria or a heavy-flavor jet produces leptons via semileptonic decay. Non-
 267 W E_T can result from mismeasurements of energy or semileptonic decays of heavy-flavor
 268 quarks. Since the E_T mismeasurement is usually not well modeled in detector simulation
 269 due to some limitations, we estimate the contribution of non- W events directly from the
 270 data sample before b -tagging is applied, known as the pretag sample.

271 Generally, the bulk of non- W events are characterized by a non-isolated lepton and small
 272 E_T . Lepton isolation I is defined as the ratio of calorimeter energy inside a cone of $\Delta R = 0.4$
 273 about the lepton to the lepton energy itself. The quantity I is small if the lepton is well-
 274 isolated from the rest of the event, as typified by a true leptonic W decay. This feature is

275 used to extrapolate the expected non- W contribution into our signal region, namely, small
276 I and large E_T . In extracting the non- W background contribution from data, we make
277 the following two assumptions: lepton isolation and E_T are uncorrelated in non- W events,
278 and the b -tagging rate is not dependent on E_T in non- W events. The level at which these
279 assumptions are justified determines the assigned uncertainty. The contributions from $t\bar{t}$ and
280 W +jets events are subtracted according to the calculated cross sections for those processes.

281 To validate the method and estimate the relevant systematic uncertainties, we vary the
282 boundaries of signal and background regions. The observed deviations imply a 25% system-
283 atic uncertainty in the non- W background yield, assigned conservatively for both the pretag
284 and tagged estimates.

285 A non- W rejection factor associated with the neural network b -tagging filter is measured
286 from data in the background region ($I > 0.2$ and $E_T > 20$ GeV), which has event kinematics
287 similar to non- W events in the signal region because lepton isolation is the only difference
288 between the two regions. The non- W estimate calculated before applying NN b -tagging
289 is scaled by this NN rejection factor; this assumes the NN filter is uncorrelated with the
290 isolation.

291 The non- W estimate for events with at least two b -tags is obtained by measuring the
292 ratio of the number of events with at least one b -tag to the number with at least two b -tags
293 in the background region and applying the ratio to the estimate of tagged non- W events in
294 the signal region.

295 For the plug region, the MET+PEM trigger is used, which causes the above-mentioned
296 method not validated due to E_T trigger bias. The E_T distribution shape difference between
297 non- W background and other backgrounds are therefore used to measure the amount of non-
298 W background. To model the non- W shape, the control samples with electron candidates
299 failed at least two of our standard lepton identification criteria are used. We perform a
300 likelihood fit for observed data using the non- W template and other background template
301 before b -tagging. The non- W contribution after b -tagging is estimated from the ratio of the
302 number after b -tagging to that before b -tagging.

304 The rate at which SECVTX falsely tags light-flavor jets is derived from inclusive jet samples
305 in varying bins of η , number of vertices, jet E_T , track multiplicity, z position of primary
306 vertex and total event E_T scalar sum. Tag rate probabilities are summed for all of the
307 taggable jets in the event, jets with at least two tracks well measured in the silicon detector.
308 Since the double-mistag rate is small, this sum is a good approximation of the single-tag
309 event rate. Negative mistags are defined as tags with unphysical negative decay length due
310 to finite tracking resolution, which assumed to be a good estimate of falsely tagged jets,
311 independent to first order of heavy flavor content in the generic jet sample. The positive
312 mistag rate can be obtained from the negative mistags with an additional correction factor,
313 reflecting an enhancement of positive mistags due to light-flavor secondary vertices and
314 material interactions in the silicon detectors. This factor is measured in inclusive jet sample
315 by fitting the asymmetry in the vertex mass distribution of positive tags over negative
316 tags [24]. The systematic uncertainty on the rate is largely due to self-consistency in the
317 parametrization as applied to the generic jet sample. The mistag rate per jet is applied
318 to events in the W +jets sample. The total estimate is corrected for the non- W QCD
319 fraction and also the top quark contributions to the pretag sample. To estimate the mistag
320 contribution in NN-tagged events, we apply the light flavor rejection power of the NN filter
321 0.35 ± 0.05 as measured using light-flavor jets from various data and simulated samples.
322 To estimate the mistag contribution in double tagged events, we apply the mistag rate to
323 all untagged jets in $W + 1 b$ -tagged jet events. In this method, the mistag contribution is
324 estimated due to a case of one real b -tag + one mistag and a double mistag case in which
325 both b -tagged jet are not real.

326 For jet probability b -tagging, the mistag rate is derived from inclusive jet samples in
327 varying bins of η , z position of the primary vertex, jet E_T , track multiplicity, number of
328 vertices and total event E_T scalar sum. The mistag rate probabilities are derived and
329 applied in the same way as for the SECVTX tag.

331 The $Wb\bar{b}$, $Wc\bar{c}$, and Wc states are major background sources of secondary vertex tags.
 332 Large theoretical uncertainties exist for the overall normalization because current Monte
 333 Carlo event generators can generate W +heavy-flavor events only to leading order. Conse-
 334 quently, rates for these processes are normalized to data. The contribution from true heavy-
 335 flavor production in W +jet events is determined from measurements of the heavy-flavor
 336 event fraction in W +jet events and the b -tagging efficiency for those events, as explained
 337 below.

338 The fraction of W +jets events produced with heavy-flavor jets has been studied ex-
 339 tensively using an ALPGEN + PYTHIA combination of Monte Carlo simulations [25, 26].
 340 Calculations of the heavy-flavor fraction in ALPGEN have been calibrated using a jet data
 341 sample, and measurements indicate a scaling factor of 1.4 ± 0.4 is necessary to make the
 342 heavy-flavor production in Monte Carlo match the production in W +1jet events. The final
 343 results of heavy-flavor fractions are obtained as shown in Table I.

344 For the tagged W +heavy flavor background estimate, the heavy-flavor fractions and
 345 tagging rates given in Tables I and II are multiplied by the number of pretag W +jets
 346 candidate events in data, after correction for the contribution of non- W and $t\bar{t}$ events to the
 347 pretag sample. The W + heavy flavor background contribution is obtained by the following
 348 relation:

$$349 \quad N_{W+HF} = f_{HF} \cdot \epsilon_{\text{tag}} \cdot [N_{\text{pretag}} \cdot (1 - f_{\text{non-}W}) - N_{\text{TOP}} - N_{\text{EWK}}], \quad (3)$$

350 where f_{HF} is the heavy-flavor fraction, ϵ_{tag} is the tagging efficiency, N_{TOP} is the expected
 351 number of $t\bar{t}$ and single top events, and N_{EWK} is the expected number of WW , WZ , ZZ
 352 and Z boson events.

353 **D. Top and Electroweak Backgrounds**

354 Production of both single top quark and top-quark pairs contribute to the tagged lep-
 355 ton+jets sample. Several electroweak boson production processes also contribute. WW
 356 pairs can decay to a lepton, neutrino as missing energy, and two jets, one of which may be
 357 charm. WZ events can decay to the signal $Wb\bar{b}$ or $Wc\bar{c}$ final state. Finally, $Z \rightarrow \tau^+\tau^-$
 358 events can have one leptonic τ decay and one hadronic decay. The leptonic τ decay gives

Jet Multiplicity	1 jet	2 jets	3 jets	≥ 4 jets
$Wb\bar{b}$ (1B) (%)	1.0 ± 0.4	2.0 ± 0.8	3.4 ± 1.4	4.6 ± 2.0
$Wb\bar{b}$ (2B) (%)	-	1.3 ± 0.6	2.5 ± 1.0	3.1 ± 1.8
$Wc\bar{c}$ (1C) (%)	7.7 ± 2.4	12.2 ± 4.5	16.4 ± 5.3	18.6 ± 6.9
$Wc\bar{c}$ (2C) (%)	-	2.0 ± 0.8	4.6 ± 1.8	8.4 ± 3.4

TABLE I: The heavy-flavor fractions, given in percent, for the $W + \text{jets}$ sample where $1B$, $2B$ refer to number of taggable b -jets in the events, with $1C$, $2C$ for charm jets. The results from ALPGEN Monte Carlo have been scaled by the data-derived calibration factor of 1.4 ± 0.4 .

Jet Multiplicity	1 jet	2 jets	3 jets	≥ 4 jets
1 SECVTX and NN b -tag (%)				
$Wb\bar{b}$ (1B)	27.5 ± 1.5	28.1 ± 1.3	26.7 ± 1.4	26.9 ± 3.7
$Wb\bar{b}$ (2B)	-	26.2 ± 1.2	24.1 ± 1.2	22.6 ± 1.3
$Wc\bar{c}$ (1C)	4.2 ± 0.2	4.6 ± 0.3	4.9 ± 0.3	5.2 ± 0.7
$Wc\bar{c}$ (2C)	-	6.3 ± 0.4	6.6 ± 0.4	6.9 ± 0.6
≥ 2 SECVTX b -tag (%)				
$Wb\bar{b}$ (2B)	-	16 ± 2	19 ± 2	19 ± 3
$Wc\bar{c}$ (2C)	-	1 ± 0	2 ± 0	2 ± 1
1 SECVTX + Jet Probability b -tag (%)				
$Wb\bar{b}$ (2B)	-	10.1 ± 1.2	11.1 ± 1.3	12.4 ± 1.5
$Wc\bar{c}$ (2C)	-	1.6 ± 0.2	2.3 ± 0.3	3.2 ± 0.4

TABLE II: The b -tagging efficiencies in percent for various b -tagging strategies on individual W +heavy-flavor processes. Categories $1B$, $2B$ refer to number of taggable b -jets in the events, with similar categories for charm jets. Those numbers include the effect of the data-to-Monte Carlo scale factors.

359 rise to a lepton + missing transverse energy, while the hadronic decay yields a narrow jet of
360 hadrons with a non-zero lifetime.

361 The normalization of the diboson and single top backgrounds are based on the theoretical

Background	Theoretical Cross Sections
WW	12.40 ± 0.80 pb
WZ	3.96 ± 0.06 pb
ZZ	1.58 ± 0.02 pb
Single top s -channel	0.88 ± 0.11 pb
Single top t -channel	1.98 ± 0.25 pb
$Z \rightarrow \tau^+\tau^-$	265 ± 30.0 pb
$t\bar{t}$	$6.7_{-0.9}^{+0.7}$ pb

TABLE III: Theoretical cross sections and uncertainties for the electroweak and single top backgrounds, along with the theoretical cross section for $t\bar{t}$ at $m_t = 175 \text{ GeV}/c^2$. The cross section of $Z^0 \rightarrow \tau^+\tau^-$ is obtained in the dilepton mass range $m_{\tau\tau} > 30 \text{ GeV}/c^2$ together with a k -factor (NLO/LO) of 1.4.

362 cross sections listed in Table III, the luminosity, and the acceptance and b -tagging efficiency
363 derived from Monte Carlo events [19, 27–29]. The acceptance is corrected for lepton identi-
364 fication, trigger efficiencies, and the z vertex cut. The tagging efficiency is always corrected
365 by the b -tagging scale factor.

366 VI. HIGGS BOSON SIGNAL ACCEPTANCE

367 The kinematics of the SM $WH \rightarrow \ell\nu b\bar{b}$ process are well defined, and events can be
368 simulated accurately by Monte Carlo generators. PYTHIA is used to generate the signal
369 samples [30]. Only Higgs boson masses between 110 and 150 GeV/c^2 are considered because
370 this is the mass region for which the decay $H \rightarrow b\bar{b}$ dominates. The number of expected
371 $WH \rightarrow \ell\nu b\bar{b}$ events N is given by

$$372 \quad N = \epsilon \cdot \int \mathcal{L} dt \cdot \sigma(p\bar{p} \rightarrow WH) \cdot \mathcal{B}(H \rightarrow b\bar{b}), \quad (4)$$

373 where ϵ , $\int \mathcal{L} dt$, $\sigma(p\bar{p} \rightarrow WH)$, and $\mathcal{B}(H \rightarrow b\bar{b})$ are the event detection acceptance, integrated
374 luminosity, production cross section, and branching fraction, respectively. The production
375 cross section and branching fraction are calculated to NLO precision [5]. The acceptance ϵ

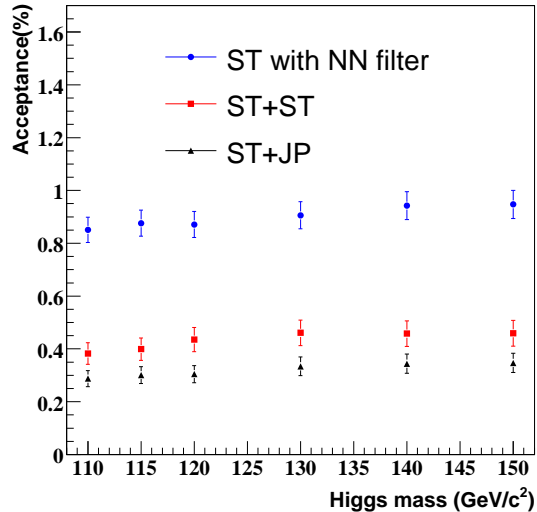


FIG. 1: The acceptance summary for the process $WH \rightarrow \ell\nu b\bar{b}$ in W+2jet bin for the selected b -tagging strategies as a function of Higgs boson mass.

376 is broken down into the following factors:

$$377 \quad \epsilon = \sum_{\ell=e,\mu,\tau} (\epsilon_{z_0} \cdot \epsilon_{\text{trigger}} \cdot \epsilon_{\text{lepton ID}} \cdot \epsilon_{b\text{tag}} \cdot \epsilon_{\text{kinematics}} \cdot \mathcal{B}(W \rightarrow \ell\nu)), \quad (5)$$

378 where ϵ_{z_0} , $\epsilon_{\text{trigger}}$, $\epsilon_{\text{lepton ID}}$, $\epsilon_{b\text{tag}}$, and $\epsilon_{\text{kinematics}}$ are efficiencies defined in sequence to meet the
 379 requirements of primary vertex, trigger, lepton identification, b -tagging, and event selection
 380 criteria. The major sources of inefficiency are the lepton identification, jet kinematics, and
 381 b -tagging factors; each is a factor between 0.3 and 0.45. The total signal acceptances for
 382 the selected b -tagging options including all systematic uncertainties as a function of Higgs
 383 boson mass are shown in Fig. 1. Including the plug electron increases the overall acceptance
 384 by 10%.

385 The expected number of signal events is estimated by Eq. 4 at each Higgs boson mass
 386 point. The expectations for the selected b -tagging strategies are shown in Table IV.

387 The total systematic uncertainty on the acceptance stems from the jet energy scale,
 388 initial and final state radiation, lepton identification, trigger efficiencies, and b -tagging scale
 389 factor. A 2% uncertainty on the lepton identification efficiency is assigned for each lepton
 390 type (CEM electron, plug electron, CMUP and CMX muon), based on studies of Z boson
 391 events. For each of the high p_T lepton triggers, a 1% uncertainty is measured from backup

b -tagging category	110 GeV	115 GeV	120 GeV	130 GeV	140 GeV	150 GeV
Pretag	9.41±0.61	7.92±0.52	6.35±0.41	3.99±0.26	2.02±0.13	0.78±0.05
ST with NN filter	2.63±0.22	2.20±0.18	1.70±0.14	1.08±0.09	0.55±0.05	0.21±0.02
ST+ST	1.18±0.14	1.00±0.12	0.85±0.10	0.55±0.07	0.27±0.03	0.10±0.01
ST+JP	0.89±0.11	0.76±0.09	0.60±0.07	0.40±0.05	0.20±0.02	0.08±0.01

TABLE IV: Expected number of $WH \rightarrow \ell\nu b\bar{b}$ signal events with systematic uncertainties for the selected b -tagging options.

b -tagging category	LeptonID	Trigger	ISR/FSR	JES	PDF	b -tagging	Total
ST with NN filter	~ 2%	< 1%	2.9%	2.3%	1.2%	3.5%	5.6%
ST+ST	~ 2%	< 1%	5.2%	2.5%	2.1%	8.4%	10.6%
ST+JP	~ 2%	< 1%	4.0%	2.8%	1.5%	9.1%	10.5%

TABLE V: Systematic uncertainties for the selected b -tagging requirements.

392 trigger paths or Z boson events. The initial and final state radiation systematic uncertainties
393 are estimated by changing the parameters related to ISR and FSR from nominal values to
394 half or double the nominal [31]. The difference from the nominal acceptance is taken as
395 the systematic uncertainty. The uncertainty in the incoming partons energies relies on the
396 eigenvectors provided in the PDF fits. An NLO version of the PDFs, CTEQ6M, provides a
397 90% confidence interval of each eigenvector [32]. The nominal PDF value is reweighted to
398 the 90% confidence level value, and the corresponding reweighted acceptance is computed.
399 The differences between nominal and reweighted acceptances are added in quadrature, and
400 the total is assigned as the systematic uncertainty [20].

401 The uncertainty due to the jet energy scale uncertainty (JES) [15] is calculated by shifting
402 jet energies in WH Monte Carlo samples by $\pm 1\sigma$. The deviation from the nominal accep-
403 tance is taken as the systematic uncertainty. The systematic uncertainty on the b -tagging
404 efficiency is based on the scale factor uncertainty discussed in Sec. IV A, IV C. When NN
405 b -tagging filter is applied, the scale factor uncertainty is added to that of SECVTX in quadra-
406 ture. The total systematic uncertainties for the selected b -tagging options are summarized
407 in Table V.

409 To improve further the signal to background discrimination after event selection, we em-
 410 ploy an artificial neural network [22] trained on a variety of kinematic variables to distinguish
 411 the W +Higgs events from backgrounds.

412 We train the neural network on the samples of simulated events using a mixture of 50%
 413 signal with $m_h = 120 \text{ GeV}/c^2$ and 50% of backgrounds. The background composition
 414 is chosen to have equal amount of $Wb\bar{b}$, $t\bar{t}$, and single top, which provides a maximum
 415 sensitivity.

416 To optimize the neural network structure, we use an iterative procedure to determine the
 417 configuration that best discriminates signal from the background, and that uses a minimal
 418 number of input discriminants. This is done by first determining the best one-variable
 419 network from a list of 76 possible variables, based on the kinematic distributions of the two
 420 jets, lepton, and E_T in the events including correlations between them. The optimization
 421 algorithm keeps this variable as an input and then loops over all other variables to determine
 422 the best two-variable network. The best N-variable network is finally selected once the
 423 N+1-variable network shows less than 0.5 percent improvement. The criteria for comparing
 424 networks is the testing error defined by how often a NN with a given configuration correctly
 425 classifies several thousand signal and background events.

426 We used the same structure of input variables to train separate neural networks for Higgs
 427 masses of 110, 115, 120, 130, 140, and 150 GeV/c^2 . Re-training networks with different
 428 signal masses keep the neural network sensitivity almost constant as function of the Higgs
 429 mass.

430 Our neural network configuration has 6 input variables, 11 hidden nodes, and 1 output
 431 node. The 6 optimal inputs are follows.

432 M_{jj+} : the invariant mass calculated from the two jets. Furthermore, if there are additional
 433 loose jets present ($E_T > 12 \text{ GeV}$ and $|\eta| < 2.4$), the loose jet that is closest to one of
 434 the two jets is included in this invariant mass calculation, if the separation between
 435 that loose jet and one of the jets is $\Delta R < 0.9$.

436 $\sum E_T(\text{Loose Jets})$: the scalar sum of the loose jet transverse energy.

437 $p_T \text{ Imbalance}$: the difference between the scalar sum of the transverse momenta of all

438 measured objects and the \cancel{E}_T . Specifically, it is calculated as $P_T(\text{jet}_1) + P_T(\text{jet}_2) +$
 439 $P_T(\text{lep}) - \cancel{E}_T$.

440 $M_{l\nu j}^{\text{min}}$: the invariant mass of the lepton, \cancel{E}_T , and one of the two jets, where the jet is
 441 chosen to give the minimum invariant mass. For this quantity, the p_z component of
 442 the neutrino is ignored.

443 $\Delta R(\text{lepton}-\nu_{\text{max}})$: the ΔR separation between the lepton and the neutrino, where the p_z
 444 of the neutrino is taken by choosing the solutions from the quadratic equations for the
 445 W mass (80.42 GeV/c²) constraint with the largest $|p_z|$.

446 $P_T(W + H)$: the total transverse momentum of the W plus two jets system, $P_T(\vec{l}ep + \vec{\nu} +$
 447 $\vec{j}et_1 + \vec{j}et_2)$.

448 All distributions are further checked and show good agreement between simulated and
 449 observed data. That confirms that our Monte Carlo modeling is adequate.

450 VIII. RESULTS

451 A. Summary of Background Estimate

452 We have described the contributions of individual background sources to the final back-
 453 ground estimate. These estimates after merging central and plug region are also plotted
 454 as a function of jet multiplicity in Figs. 2, separately for single and double b -tagging cate-
 455 gories. The background estimates of 2 jet events for the three tagging categories are also
 456 summarized in Tables VI, VII and VIII for the central lepton and plug lepton region, re-
 457 spectively. The observed number of events in the data and the SM background expectations
 458 are consistent in each b -tagging condition.

459 B. Limit on Higgs Boson Production Rate

460 We apply the neural network to the samples of simulated events and obtain the distribu-
 461 tions of the network output for all the processes considered. After weighting their expected
 462 event yields the resulting distributions are compared to the data observed in single and dou-
 463 ble b -tagging categories as shown in Fig. 3. We use a binned likelihood technique to fit the

	Central region	Plug region
Njet	2jet	
Pretag Events	32242	5879
Mistag	107.1±9.38	28.47±3.30
$Wb\bar{b}$	215.6±92.34	43.09±12.33
$Wc\bar{c}$	167.0±62.14	33.37±9.55
$t\bar{t}$ (6.7pb)	60.68±9.30	7.17±1.00
Single top(s-ch)	14.38±2.09	1.53±0.20
Single top(t-ch)	29.57±4.33	3.54±0.47
WW	15.45±1.91	3.00±0.20
WZ	7.59±0.81	1.62±0.09
ZZ	0.31±0.03	0.02±0.00
$Z \rightarrow \tau\tau$	7.27±1.12	0.24±0.03
nonW QCD	184.7±33.04	18.34±5.54
Total Bkg	809.61±159.38	140.4±16.9
WH signal (120 GeV)	1.70±0.14	0.20±0.01
Observed Events	805	138

TABLE VI: Background estimate for events with exactly one SECVTX b -tag that passes the NN b -tagging filter.

464 observed neural network distributions in three b -tagging categories to test for the presence
465 of a WH signal. No excess over the background is observed. We therefore proceed to set an
466 upper limit on the WH production cross section times $H \rightarrow b\bar{b}$ branching fraction.

467 The number of events in each bin follows the Poisson distribution

$$468 \quad P_i(n_i, \mu_i) = \frac{\mu_i^{n_i} e^{-\mu_i}}{n_i!} \quad (i = 1, 2, \dots, N_{\text{bin}}), \quad (6)$$

469 where n_i , μ_i , and N_{bin} represent the number of observed events in the i -th bin, the expectation
470 in the i -th bin, and the total number of bins. The Higgs production hypothesis is constructed
471 by setting μ_i to $\mu_i = s_i + b_i$, where s_i and b_i are the number of signal and expected background

	Central region	Plug region
Njet	2jet	
Pretag Events	32242	5879
Mistag	3.88±0.35	1.00±0.18
$Wb\bar{b}$	37.93±16.92	7.40±3.96
$Wc\bar{c}$	2.88±1.25	0.96±0.49
$t\bar{t}(6.7\text{pb})$	19.05±2.92	2.14±0.34
Single top(s-ch)	6.90±1.00	0.69±0.10
Single top(t-ch)	1.60±0.23	0.22±0.04
WW	0.17±0.02	0.01±0.01
WZ	2.41±0.26	0.58±0.06
ZZ	0.06±0.01	0.00±0.00
$Z \rightarrow \tau\tau$	0.25±0.04	0.00±0.00
nonW QCD	5.50±1.00	1.16±0.44
Total Bkg	80.62±18.75	14.18±4.03
WH signal (120 GeV)	0.85±0.10	0.09±0.01
Observed Events	83	11

TABLE VII: Background estimate for events with at least two SECVTX b -tagged jets.

472 events in the i -th bin. This quantity s_i can also be written as a product

$$473 \quad s_i = \sigma(p\bar{p} \rightarrow W^\pm H) \cdot \mathcal{B}(H \rightarrow b\bar{b}) \cdot \epsilon_{WH} \cdot \int \mathcal{L} dt \cdot f_i^{WH}, \quad (7)$$

474 where f_i^{WH} is the fraction of the total signal which lies in the i -th bin. In this case, $\sigma(p\bar{p} \rightarrow$
475 $W^\pm H) \cdot \mathcal{B}(H \rightarrow b\bar{b})$ is the variable to be extracted from data. An upper limit on the Higgs
476 boson production cross section times branching fraction $\sigma(p\bar{p} \rightarrow W^\pm H) \cdot \mathcal{B}(H \rightarrow b\bar{b})$ is
477 extracted by using a Bayesian procedure.

478 The likelihoods from the three b -tagging categories are multiplied together. The system-
479 atic uncertainties associated with the pretag acceptance, luminosity uncertainty, and uncer-
480 tainty of the b -tagging efficiency scale factor are considered to be fully correlated between the
481 three selection channels. Background uncertainties, specifically on the heavy-flavor fractions
482 and b -tagging scale factor, are also completely correlated. The effect of shape systematic

	Central region	Plug region
Njet	2jet	
Pretag Events	32242	5879
Mistag	11.73±0.92	3.18±0.49
$Wb\bar{b}$	31.15±14.03	6.23±3.37
$Wc\bar{c}$	7.87±3.43	1.53±0.81
$t\bar{t}$ (6.7pb)	15.56±2.39	1.79±0.31
Single top(s-ch)	5.14±0.75	0.51±0.08
Single top(t-ch)	1.87±0.27	0.24±0.04
WW	0.93±0.11	0.12±0.04
WZ	1.84±0.20	0.42±0.05
ZZ	0.08±0.01	0.01±0.00
$Z \rightarrow \tau\tau$	1.29±0.20	0.01±0.00
nonW QCD	9.55±1.73	1.51±0.55
Total Bkg	86.99±17.99	15.54±3.56
WH signal (120 GeV)	0.60±0.07	0.06±0.01
Observed Events	90	13

TABLE VIII: Background estimate for events with one SECVTX plus Jet probability b -tagged jets.

483 uncertainties on the network output are also studied and found to have a negligible impact
484 on the final results. We assume an uniform prior probability for $\sigma \cdot \mathcal{B}$ and integrate the
485 likelihood over all parameters except $\sigma \cdot \mathcal{B}$. A 95% credibility level upper limit on $\sigma \cdot \mathcal{B}$ is
486 obtained by calculating the 95th percentile of the resulting distributions.

487 To measure the expected sensitivity for this analysis, background-only pseudo-
488 experiments are used to calculate an expected limit in the absence of Higgs boson production.
489 Pseudo-data are generated by fluctuating the individual background estimates within total
490 uncertainties. The expected limit is derived from the median of 95% confidence level upper
491 limit of the one thousand pseudo-data using Eq. 9.

492 The observed limits as a function of the Higgs boson mass are shown in Fig. 4 and

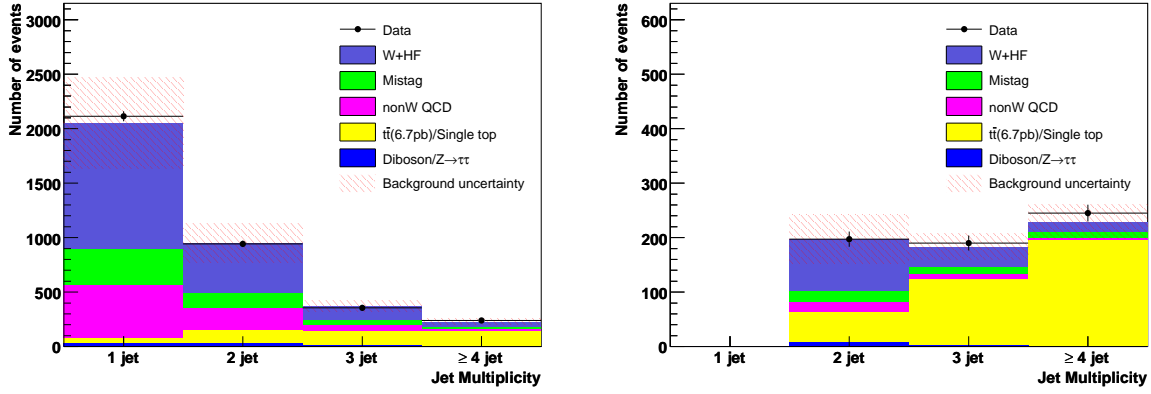


FIG. 2: Number of events as a function of jet multiplicity for events with exactly one SECVTX b -tag applying the NN b -tagging filter requirement (left) and for events with at least two SECVTX b -tagged jets or one SECVTX b -tagged jet plus one jet probability b -tagged jet (right).

Higgs Mass GeV/ c^2	Upper Limit (pb)		Upper Limit/SM	
	Observed	Expected	Observed	Expected
110	1.2	1.2	7.5	7.8
115	1.2	1.1	9.0	8.7
120	1.1	1.1	10.2	10.5
130	1.1	0.9	17.9	15.2
140	1.2	0.8	40.1	28.7
150	1.1	0.8	101.9	70.9

TABLE IX: Observed and expected upper limits on $\sigma(p\bar{p} \rightarrow WH) \cdot \mathcal{B}(H \rightarrow b\bar{b})$ at 95 % C.L. compared to the SM production rate calculated at NNLO.

493 Table IX, together with the expected limits determined from pseudo-experiments. The
494 search sensitivity is improved significantly with respect to previous searches, about 60%
495 beyond the expectations from simple luminosity scaling. The main improvements are using
496 Jet Probability b -tagging, an multivariate neural network technique, and leptons in the
497 forward region.

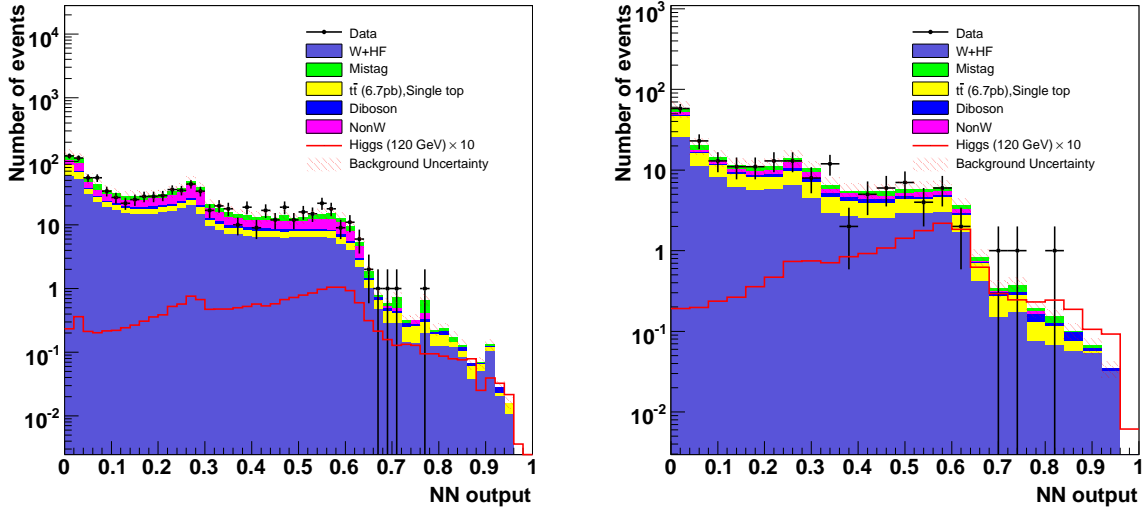


FIG. 3: Neural Network output distribution in $W+2$ jets events for exactly one SECVTX b -tagged jet that passes the NN b -tagging filter (left) and events for ST+ST and ST+JP double b -tagging categories (right). The contributions of the various background sources from the central plus plug region are shown in histograms while the hatched box represents the background uncertainty.

498 IX. CONCLUSIONS

499 We have presented a search for the standard model Higgs boson in the $\ell\nu b\bar{b}$ final state
500 expected from WH production. The candidate events are separated into three b -tagging
501 categories and optimized for this search. In addition, the forward lepton region is included
502 to increase the signal acceptance. Finally, a neural network technique is applied to provide
503 additional discrimination between signal and background sources. This improvement, along
504 with a total dataset corresponding to 1.9 fb^{-1} , allows us to improve the upper limit on Higgs
505 boson production. We set a 95% confidence level upper limit on the production cross section
506 times branching fraction that ranges from 1.2 to 1.1 pb or 7.5 to 101.9 times the Standard
507 Model expectation for Higgs boson masses spanning 110 to $150 \text{ GeV}/c^2$.

508 Acknowledgments

509 We thank the Fermilab staff and the technical staffs of the participating institutions for
510 their vital contributions. This work was supported by the U.S. Department of Energy and

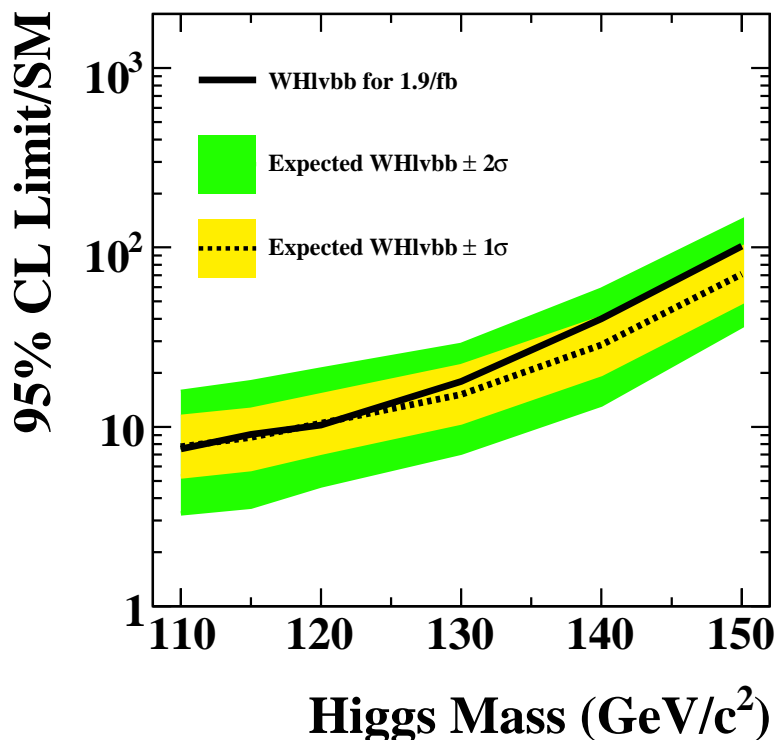


FIG. 4: 95% confidence level upper limit on $\sigma(p\bar{p} \rightarrow WH) \cdot \mathcal{B}(H \rightarrow b\bar{b})$ relative to the SM expectations with an integrated luminosity of 1.9 fb^{-1} obtained from the likelihood combined central and plug lepton region with three b -tagging conditions. Solid line indicate 95% confidence level upper limit obtained from data and dashed line indicates 95% confidence level upper limit calculated by the median of one thousand pseudo-experiments.

511 National Science Foundation; the Italian Istituto Nazionale di Fisica Nucleare; the Min-
512 istry of Education, Culture, Sports, Science and Technology of Japan; the Natural Sciences
513 and Engineering Research Council of Canada; the National Science Council of the Republic
514 of China; the Swiss National Science Foundation; the A.P. Sloan Foundation; the Bun-
515 desministerium für Bildung und Forschung, Germany; the Korean Science and Engineering
516 Foundation and the Korean Research Foundation; the Particle Physics and Astronomy Re-
517 search Council and the Royal Society, UK; the Institut National de Physique Nucleaire et
518 Physique des Particules/CNRS; the Russian Foundation for Basic Research; the Comisión
519 Interministerial de Ciencia y Tecnología, Spain; the European Community's Human Poten-

- 521 [1] P. W. Higgs, *Phys. Rev. Lett.* **13**, 508 (1964).
- 522 [2] R. Barate et al. (ALEPH, DELPHI, L3, and OPAL collaborations and the LEP Working
523 Group for Higgs boson searches), *Phys. Lett.* **B565**, 61 (2003), hep-ex/0306033.
- 524 [3] J. Alcaraz et al. (ALEPH, DELPHI, L3, and OPAL collaborations and the LEP Electroweak
525 Working Group), Tech. Rep. CERN-PH-EP-2006-042 (2006), hep-ex/0612034.
- 526 [4] T. Han and S. Willenbrock, *Phys. Lett.* **B273**, 167 (1991).
- 527 [5] A. Djouadi, J. Kalinowski, and M. Spira, *Comput. Phys. Commun.* **108**, 56 (1998), hep-
528 ph/9704448.
- 529 [6] A. Abulencia et al. (CDF collaboration), *Phys. Rev.* **D75**, 012010 (2007), hep-ex/0612015.
- 530 [7] T. Aaltonen et al. (CDF), *Phys. Rev. Lett.* **100**, 041801 (2008), 0710.4363.
- 531 [8] T. Aaltonen et al. (CDF), *Phys. Rev.* **D78**, 032008 (2008), 0803.3493.
- 532 [9] V. M. Abazov et al. (D0 collaboration), *Phys. Lett. B* **663**, 26 (2008), hep-ex/0712.0598.
- 533 [10] D. Acosta et al. (CDF collaboration), *Phys. Rev.* **D71**, 032001 (2005), hep-ex/0412071.
- 534 [11] L. Balka et al., *Nucl. Instrum. Methods* **A267**, 272 (1988).
- 535 [12] S. Bertolucci et al., *Nucl. Instrum. Methods* **A267**, 301 (1988).
- 536 [13] M. G. Albrow et al., *Nucl. Instrum. Methods* **A480**, 524 (2002).
- 537 [14] F. Abe et al. (CDF collaboration), *Phys. Rev.* **D45**, 1448 (1992).
- 538 [15] A. Bhatti et al., *Nucl. Instrum. Methods* **A566**, 375 (2006), hep-ex/0510047.
- 539 [16] G. Ascoli et al., *Nucl. Instrum. Methods* **A268**, 33 (1988).
- 540 [17] T. Dorigo (CDF collaboration), *Nucl. Instrum. Methods* **A461**, 560 (2001).
- 541 [18] E. J. Thomson et al., *IEEE Trans. Nucl. Sci.* **49**, 1063 (2002).
- 542 [19] D. Acosta et al. (CDF collaboration), *Phys. Rev. Lett.* **94**, 091803 (2005), hep-ex/0406078.
- 543 [20] D. Acosta et al. (CDF collaboration), *Phys. Rev.* **D71**, 052003 (2005), hep-ex/0410041.
- 544 [21] A. Abulencia et al. (CDF collaboration), *Phys. Rev. Lett.* **97**, 082004 (2006).
- 545 [22] C. Peterson, T. Rönngvaldsson, and L. Lönnblad, *Comput. Phys. Commun.* **81**, 185 (1994).
- 546 [23] A. Abulencia et al. (CDF collaboration), *Phys. Rev.* **D74**, 072006 (2006), hep-ex/0607035.
- 547 [24] A. Abulencia et al. (CDF collaboration), *Phys. Rev. Lett.* **97**, 082004 (2006), hep-ex/0606017.
- 548 [25] M. L. Mangano, M. Moretti, F. Piccinini, R. Pittau, and A. D. Polosa, *J. High Energy Phys.*

- 549 **07**, 001 (2003), hep-ph/0206293.
- 550 [26] G. Corcella et al. (2001), hep-ph/0201201.
- 551 [27] J. Campbell and R. K. Ellis, Phys. Rev. **D65**, 113007 (2002), hep-ph/0202176.
- 552 [28] M. Cacciari, S. Frixione, M. L. Mangano, P. Nason, and G. Ridolfi, J. High Energy Phys. **04**,
553 068 (2004), hep-ph/0303085.
- 554 [29] B. W. Harris, E. Laenen, L. Phaf, Z. Sullivan, and S. Weinzierl, Phys. Rev. **D66**, 054024
555 (2002), hep-ph/0207055.
- 556 [30] T. Sjöstrand et al., Comput. Phys. Commun. **135**, 238 (2001), hep-ph/0010017.
- 557 [31] A. Abulencia et al. (CDF collaboration), Phys. Rev. **D73**, 032003 (2006), hep-ex/0510048.
- 558 [32] J. Pumplin et al., J. High Energy Phys. **07**, 012 (2002), hep-ph/0201195.